PHYSICAL REVIEW B **76**, 205301 (2007)

Dependence of spin dephasing on initial spin polarization in a high-mobility two-dimensional electron system

D. Stich,[1] J. Zhou,[2] T. Korn,[1] R. Schulz,[1] D. Schuh,[1] W. Wegscheider,[1] M. W. Wu,[2,*] and C. Schüller[1,†]
[1]*Institut für Experimentelle und Angewandte Physik, Universität Regensburg, D-93040 Regensburg, Germany*
[2]*Hefei National Laboratory for Physical Sciences at Microscale and Department of Physics, University of Science and Technology of China, Hefei, Anhui, 230026, China*
(Received 27 July 2007; published 1 November 2007)

We have studied the spin dynamics of a high-mobility two-dimensional electron system in a $GaAs/Al_{0.3}Ga_{0.7}As$ single quantum well by time-resolved Faraday rotation and time-resolved Kerr rotation in dependence on the initial degree of spin polarization, P, of the electrons. By increasing the initial spin polarization from the low-P regime to a significant P of several percent, we find that the spin dephasing time, T_2^*, increases from about 20 to 200 ps. Moreover, T_2^* increases with temperature at small spin polarization but decreases with temperature at large spin polarization. All these features are in good agreement with theoretical predictions by Weng and Wu [Phys. Rev. B **68**, 075312 (2003)]. Measurements as a function of spin polarization at fixed electron density are performed to further confirm the theory. A fully microscopic calculation is performed by setting up and numerically solving the kinetic spin Bloch equations, including the D'yakonov-Perel' and the Bir-Aronov-Pikus mechanisms, with *all* the scattering explicitly included. We reproduce all principal features of the experiments, i.e., a dramatic decrease of spin dephasing with increasing P and the temperature dependences at different spin polarizations.

DOI: 10.1103/PhysRevB.76.205301 PACS number(s): 73.20.−r, 39.30.+w, 85.75.−d, 71.70.Ej

I. INTRODUCTION

In the past decade, the spin degrees of freedom in semiconductors have been investigated both experimentally and theoretically due to the great prospect of potential applications in spintronics or quantum computational devices.[1,2] Unaffectedly, the study of spin dephasing/relaxation has been one of the most important and interesting branches of this field. The dominant spin dephasing mechanism in n-doped GaAs quantum wells (QWs) is the D'yakonov-Perel' (DP) mechanism.[4] It is caused by the k-vector dependent effective magnetic fields which arise from the bulk inversion asymmetry[5] (BIA) and the structure inversion asymmetry (SIA).[6] Electrons with different k-vectors experience different effective magnetic fields $\mathbf{B}(k)$, and they would precess at different frequency Ω. By averaging the magnitude of $\mathbf{B}(k)$ over the momentum distribution of the electrons, an average Larmor frequency Ω_{av} due to the effective magnetic fields can be determined. For the DP mechanism, two limiting cases are considered:[2,3] (i) $\tau_p\Omega_{\mathrm{av}} \geqslant 1$: If the product of average Larmor frequency Ω_{av} and momentum relaxation time τ_p is larger than one, spins may precess more than a full cycle before being scattered into another momentum state. Strong interference induced decay happens in this limit. (ii) $\tau_p\Omega_{\mathrm{av}} \leqslant 1$: In this regime, the momentum relaxation time τ_p is so short that the effective magnetic field $\mathbf{B}(k)$ may be treated as a rapid fluctuation. Individual electron spins only precess by a fraction of a full cycle before the effective magnetic field changes amplitude and direction due to momentum scattering. In this regime, the spin dephasing time τ_s is inversely proportional to the momentum relaxation time τ_p. This behavior is commonly called motional narrowing.

In a number of experiments performed by Kikkawa *et al.*,[7,8] extremely long spin relaxation times could be achieved in GaAs bulk material[7] or in II-VI quantum wells[8] by using doping levels close to the metal-insulator transition. The spin dephasing close to the metal-insulator transition was further studied by Sandhu *et al.*[9] The dopants act as centers of momentum scattering that enhance spin lifetime due to motional narrowing. On one hand, this is helpful for manipulation of optically excited spins. On the other hand, however, a high impurity density is undesirable for a transistor device, where highly-mobile charge carriers are required with dissipation processes as low as possible. Most proposals for spin transistor device structures are within the ballistic regime and thus require extremely high mobility. Recently, however, Schliemann *et al.* introduced a concept for a spin transistor device working in the diffusive transport regime.[10] Measurements of the spin dephasing in modulation n-doped quantum wells have so far focused on structures grown in the [110] crystal direction, in which Ohno *et al.* found spin dephasing times of several nanoseconds.[11] These are due to the fact that in a [110]-grown QW, the Dresselhaus spin-orbit field points along the growth direction for electrons of arbitrary k vector. For electron spins aligned along the [110] direction, the DP mechanism is thus absent, as the spins are parallel to the Dresselhaus field and do not precess. As soon as a magnetic field is applied in the sample plane, however, the spins are forced to precess and change their orientation. This leads to a drastic decrease of the spin dephasing time (SDT), shown theoretically by Wu and Kuwata-Gonokami[12] and experimentally by Döhrmann *et al.*[13] This is because for spins with an orientation different from [110], the Dresselhaus field again causes a precessional motion, leading to dephasing due to the DP mechanism. From the point of view of applications, the advantage of long spin dephasing time in [110]-grown QWs is thus diminished, as the manipulation of spins by an external magnetic field destroys it. This is also the case for electrical fields applied in the growth direction, either by asymmetric modulation doping of the QW, or by an external

gate voltage. This is due to the fact that an electrical field induces a structural inversion asymmetry, which manifests itself in the Rashba spin-orbit term in the Hamiltonian. Like the Dresselhaus term, it may be described by a k-dependent effective magnetic field. For the [110]-grown QW, the Rashba field direction is within the sample plane, thus causing spin dephasing even for spins aligned in the [110] direction. Karimov *et al.* demonstrated that the SDT in a [110]-grown QW may be decreased by an order of magnitude by applying an electrical field in the growth direction which effectively tunes the contribution of the Rashba field to spin dephasing.[14]

In high-mobility two-dimensional electron systems (2DES), electron-electron Coulomb interaction can play an important role. It was first pointed out by Wu and Ning[15] that any scattering including the spin conserving Coulomb scattering can cause an irreversible spin dephasing in the presence of inhomogeneous broadening. This inhomogeneous broadening can be from the energy-dependent g factor,[15] the Dresselhaus-Rashba terms,[16] and even the k-dependent spin diffusion along a spacial gradient.[17] Recently, also for [001]-grown n-doped QWs, the importance of the electron-electron scattering for spin relaxation and dephasing was proved by Glazov and Ivchenko[18] by using perturbation theory and by Weng and Wu[19] from a fully microscopic many-body approach. In a thorough temperature-dependence study of the spin dephasing in [001]-oriented n-doped QWs, Leyland *et al.* experimentally verified the effects of the electron-electron scattering.[20] In almost all theoretical and experimental investigations, the spin polarization is very small and there is no/small external electric field parallel to the QWs. In other words, the spin systems are near the equilibrium. Nevertheless, Wu *et al.* set up the kinetic spin Bloch equations which can be used to investigate the spin kinetics regardless of how far away from the equilibrium.[19,21–23] While numerically solving these equations, all the scatterings such as electron-acoustic phonon, electron-longitudinal phonon, electron-nonmagnetic impurity, and especially the electron-electron Coulomb scatterings are explicitly included.[19,23,24] Weng and Wu predicted an interesting effect that the spin dephasing is greatly suppressed by increasing the initial spin polarization in Ref. 19. This effect comes from the Hartree-Fock (HF) term of the Coulomb interaction. This term serves as an effective magnetic field along the z axis which can be greatly increased with the spin polarization and therefore blocks the spin precession as a result of the lack of detuning.[19] Moreover, they further predicted that for high mobility samples, the spin dephasing time decreases with temperature at high spin polarization, which is in *opposite* to the case of small polarization.[19]

Here, we report on time-resolved experiments in which we manage to realize a significant spin polarization and indeed observe the proposed effects. Spin-polarized carriers are injected into the 2DES at the Fermi level by way of optical pumping with a circularly-polarized laser. The SDT T_2^* is determined through time-resolved Faraday rotation (TRFR) and time-resolved Kerr rotation (TRKR). We find that T_2^* visibly increases with increasing initial spin polarization and it increases/decreases with temperature at small/large spin polarization. All these features are in good agreement with the theoretical predictions.[19] In addition, we present the effect of spin-conserving and spin-flip electron-heavy hole scattering, and the screening from the hole gas on spin dephasing. Control experiments using constant excitation density and varying the circular polarization degree of the pump beam demonstrate that the observations are due to an increased initial spin polarization instead of caused by either increased electron density or changes in sample temperature. Moreover, the variation of the electron g factor with degree of spin polarization has the same tendency both in experiment and theory.

This paper is organized as following. In Sec. II, we construct the kinetic spin Bloch equations. Then we describe the preparation of the sample in Sec. III. The setup of the experiment and the main results both in experiments and calculations are presented in Sec. IV. We conclude in Sec. V.

II. MICROSCOPIC CALCULATIONS

First, we construct the kinetic spin Bloch equations in GaAs QWs by using the nonequilibrium Green's function method:[25]

$$\dot{\rho}_{\mathbf{k},\sigma\sigma'} = \dot{\rho}_{\mathbf{k},\sigma\sigma'}|_{\mathrm{coh}} + \dot{\rho}_{\mathbf{k},\sigma\sigma'}|_{\mathrm{scatt}}, \tag{1}$$

with $\rho_{\mathbf{k},\sigma\sigma'}$ representing the single particle density matrix elements. The diagonal and off-diagonal elements of $\rho_{\mathbf{k},\sigma\sigma'}$ give the electron distribution functions $f_{\mathbf{k}\sigma}$ and the spin coherence $\rho_{\mathbf{k},\sigma-\sigma}$, respectively. The coherent terms $\dot{\rho}_{k,\sigma\sigma'}|_{\mathrm{coh}}$ describe the precession of the electron spin due to the effective magnetic field from the Dresselhaus term[34] $\Omega^{\mathrm{BIA}}(\mathbf{k})$, the Rashba term $\Omega^{\mathrm{SIA}}(\mathbf{k})$, and the HF term of Coulomb interaction. The expressions of the coherent term can be found in Refs. 19 and 23. The Dresselhaus term can be written as[26] $\Omega_x^{\mathrm{BIA}}(\mathbf{k})=\gamma k_x(k_y^2-\langle k_z^2\rangle)$, $\Omega_y^{\mathrm{BIA}}(\mathbf{k})=\gamma k_y(\langle k_z^2\rangle-k_x^2)$, and, $\Omega_z^{\mathrm{BIA}}(\mathbf{k})=0$, in which $\langle k_z^2\rangle$ represents the average of the operator $-(\partial/\partial z)^2$ over the electronic state of the lowest subband.[24] γ is the spin splitting parameter,[27] and we choose it to be 17.1 eV Å^3 all through the paper. The Rashba term can be written as $\Omega_x^{\mathrm{SIA}}(\mathbf{k})=\alpha k_y$, $\Omega_y^{\mathrm{SIA}}(\mathbf{k})=-\alpha k_x$, and, $\Omega_z^{\mathrm{SIA}}(\mathbf{k})=0$, in which the Rashba spin-orbit parameter α is proportional to the interface electric field, and we choose it to be $0.65\gamma\langle k_z^2\rangle$ according to our experiment of magnetoanisotropy of electron spin dephasing.[28] $\dot{\rho}_{k,\sigma\sigma'}|_{\mathrm{scatt}}$ in Eq. (1) denote the electron-LO-phonon, electron-AC-phonon, electron-nonmagnetic impurity, and the electron-electron Coulomb scatterings whose expressions are given in detail in Refs. 19, 23, and 24. Moreover, we further include the spin-conserving and spin-flip electron-heavy-hole scatterings whose expressions are given in detail in Ref. 29. The latter one leads to the so-called Bir-Aronov-Pikus (BAP) spin dephasing.[30]

After numerically solving the kinetic spin Bloch equations self-consistently, one can obtain the spin relaxation and dephasing times from the temporal evolutions of the electron distributions and the spin coherence.[22]

III. SAMPLE GROWTH AND PREPARATION

Our sample was grown by molecular beam epitaxy on a [001]-oriented semi-insulating GaAs substrate. The active

region is a 20-nm-wide, one-sided modulation-doped GaAs-$Al_{0.3}Ga_{0.7}As$ single QW. The electron density and mobility at $T=4.2$ K are $n_e=2.1\times10^{11}$ cm^{-2} and $\mu_e=1.6\times10^6$ cm^2/V s, respectively. These values were determined by transport measurements on an unthinned sample. For measurements in transmission geometry, the sample was glued onto a glass substrate with an optical adhesive, and the substrate and buffer layers were removed by selective etching.

IV. TIME-RESOLVED KERR AND FARADAY ROTATION

A. Experimental setup

For both, the TRFR and the TRKR measurements, two laser beams from a mode-locked Ti:sapphire laser, which is operated at 80 MHz repetition rate, were used. The laser pulses had a temporal length of about 600 fs each, resulting in a spectral width of about 3–4 meV, which allowed for a resonant excitation. The laser wavelength was tuned to excite electrons from the valence band to states slightly above the Fermi energy of the host electrons in the conduction band. Both laser beams were focused to a spot of approximately 60 μm diameter on the sample surface. The pump pulses were circularly polarized by an achromatic $\lambda/4$ plate in order to create spin-oriented electrons in the conduction band, with spins aligned perpendicular to the QW plane. The TRFR measurements were performed in a split-coil magnet cryostat with a ^{3}He insert, allowing for sample temperatures between 1.5 and 4.5 K. The TRKR measurements were performed in a continuous-flow He cold finger cryostat. In this cryostat, nonthinned samples from the same wafer were used. Unless otherwise stated, the experiments were carried out at a nominal sample temperature of $T=4.5$ K.

Average pump powers between about 100 μW and 6 mW were used to create different densities, n_{ph}, of photoexcited, spin-aligned electrons. The energy-dependent absorption coefficient of the sample and the laser spot size were measured. Together with the laser beam intensity, we estimated the total densities, $n_{\mathrm{ph}}^{\mathrm{tot}}$, of electron-hole pairs, to be between about $n_{\mathrm{ph}}^{\mathrm{tot}}=9\times10^9$ cm^{-2} for the lowest, and $n_{\mathrm{ph}}^{\mathrm{tot}}=6\times10^{11}$ cm^{-2} for the highest pump intensities. Referring to $k\cdot p$ calculations of Pfalz *et al.*,[31] we have determined for our 20-nm-wide GaAs well the densities of spin-aligned electrons n_{ph} by multiplying $n_{\mathrm{ph}}^{\mathrm{tot}}$ by a factor of 0.4 to account for heavy-hole/light-hole mixing in the valence band. The resulting maximal degree of initial spin polarization of electrons, P_m, was then calculated via the relation

$$P_m = n_{\mathrm{ph}}/(n_e + n_{\mathrm{ph}}^{\mathrm{tot}}). \tag{2}$$

We emphasize that this value represents an upper boundary for the initial spin polarization. In the experiment, the maximum overlap of pump and probe beam is typically not at the beam waist, thus we generally probe a somewhat lower density/initial spin polarization than estimated by Eq. (2). In comparing the experiment to numerical calculations, the initial spin polarization, P, is thus used as a fitting parameter. As will be shown below, we consistently found slightly lower values of P, as compared to the experimentally estimated P_m. The intensity of the linearly polarized probe pulses was kept constant at an average power of about 0.5 mW, and the rotation of the probe polarization due to the Faraday/Kerr effect was measured by an optical bridge.

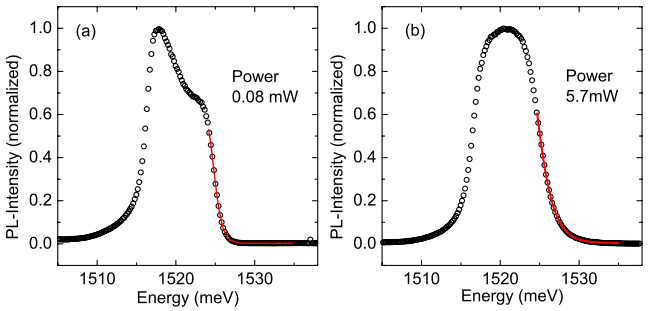

FIG. 1. (Color online) (Open circles) Power-dependent PL spectra measured with a grating spectrometer. The local temperature at the laser focus spot was determined by fitting the Fermi-Dirac distribution function to the high-energy tail of the PL (red line). (a) PL spectrum and fit for low pump fluence of 0.08 mW. The corresponding local temperature is 6.7±1 K. (b) PL spectrum and fit for high pump fluence of 5.7 mW. The corresponding local temperature is 16±2 K.

B. Absorption and power-dependent photoluminescence measurements

In the TRFR and TRKR measurements, various pump beam fluences are used to create different initial values of the spin polarization. As the pump beam fluence is increased, an increased amount of power is deposited in the laser focus spot, locally increasing the sample temperature. In order to calibrate our measurements and the corresponding calculations, a local probe of the sample temperature at the measurement spot is necessary. We utilize power-dependent photoluminescence (PL) measurements to determine the local sample temperature. For this, the sample is excited by tuning the pulsed Ti:sapphire laser to slightly higher (by 14 meV) photon energies than during the TRFR and TRKR measurements. In this spectral range, the absorption coefficient of the QW is almost constant, as determined by white-light absorption measurements. This enables us to observe the PL emitted from the 2DES with a grating spectrometer under conditions that closely resemble those during the time-resolved measurements.

To extract the local temperature from the PL data, a Fermi-Dirac distribution is fitted to the high-energy tail of the PL, which corresponds to the recombination of electrons at the Fermi energy. Figure 1 shows the PL data (open circles) and the fits (red lines) for the cases of low and high pump beam fluence. In Fig. 1(a), where a low pump fluence is used, we observe the typical, triangular shape of the PL signal from a high-mobility 2DES, with a sharp cutoff of PL intensity for values above the Fermi energy. In Fig. 1(b), corresponding to a large pump beam fluence, the high-energy tail is far more rounded, indicating a higher local temperature.

C. Zero-field coherent spin oscillations

Figure 2(b) shows two TRFR traces taken at *zero* external magnetic field for low pump beam fluence. The upper trace,

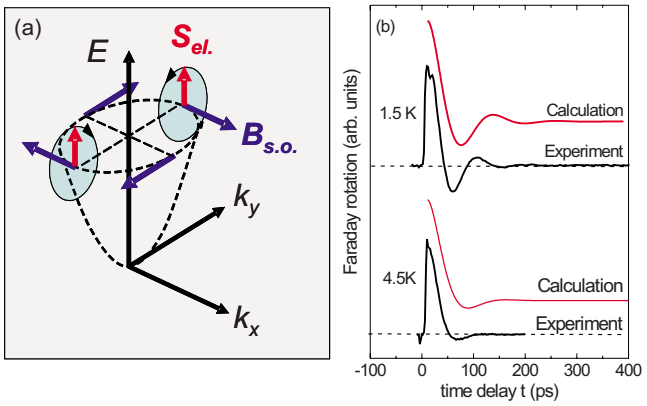

FIG. 2. (Color online) (a) Schematic of the geometry of the Rashba spin-orbit field for the [001]-grown QW. For electrons at the Fermi energy, while the direction of the Rashba field varies within the $x-y$ plane, its magnitude is constant. Thus the z component of the electron spins performs a coherent oscillation. (b) TRFR traces at low excitation density taken at two different temperatures. For the lower temperature, a coherent oscillation at *zero* magnetic field is clearly observed. (c) Calculated spin decay curves for these two temperatures.

measured at a sample temperature of 4.5 K, shows a strongly damped oscillation of the TRFR signal. In the lower trace, taken at a reduced sample temperature of about 1.5 K under otherwise identical conditions, this damped oscillation is much more pronounced. The oscillatory signal is due to a coherent oscillation of the excited electron spins about an effective spin-orbit field caused by k-linear terms in the Rashba-Dresselhaus Hamiltonian. Figure 2(a) illustrates this schematically for a pure Rashba field: electrons are created at the Fermi energy by the pump laser pulse, with their spins initially aligned along the growth direction. While their k vectors have arbitrary direction in the $x-y$ plane, they have the same magnitude. The individual Rashba fields for these electrons are all in-plane with the same magnitude, causing the electron spins to precess into the sample plane with equal Larmor frequencies. The observed oscillation of the TRFR signal is the coherent sum of the z component of the individual spins oscillating about their individual Rashba-Dresselhaus fields. This coherent oscillation has already been observed experimentally[32] and is representative of the weak scattering limit. We note that the amplitude of the effective Rashba-Dresselhaus field, calculated from the oscillation frequency using the in-plane electron g factor $|g|=0.355$, is $B_{\text{eff}}=2.35$ T. The red lines in Fig. 2(b) present the calculated temporal evolutions of the differences of spin-up and -down electron densities (normalized ΔN) for the two corresponding cases. One can see that the damped oscillation is indeed pronounced for lower temperature. Furthermore, the oscillation period is very sensitive to the strength of Rashba-Dresselhaus spin-orbit coupling and electron momentum scattering time. Therefore, it is understandable that the calculated oscillation period is a little different from the experiment as all the parameters we used are fixed.

D. Dependence of SDT on initial spin polarization

Figure 3(a) shows a series of TRFR traces taken for different pump beam fluences and thus different initial values of the spin polarization. For all TRFR traces, a very fast decay of the TRFR signal is observed during the first few picoseconds after excitation. We attribute this to the spin polarization of the photoexcited holes, which typically lose their initial spin orientation extremely fast. A second, significantly slower decaying part of the signal is attributed to the spin dephasing of the photoexcited electrons. Using a biexponential fit function, the SDT is determined from the data. It is clearly visible that with increasing spin polarization, the SDT increases as well, from about 20 ps to more than 200 ps. This observation is in good agreement with predictions by Weng and Wu,[19] which stem from their fully microscopic calculations. It has been mentioned above that the estimated value of initial spin polarization, P_m, in Eq. (2) is an upper boundary. Therefore, the polarization values we used in Ref. 35 [cf. Fig. 3(a)] are actually larger than the real ones. For this reason, we introduced in Ref. 35 a fitting parameter τ to obtain the same T_2^* as the experiment. In this paper, we choose the initial spin polarization P as a fitting parameter instead of introducing τ. This seems to be more reasonable, since, as mentioned above, the experimentally determined P_m is just an upper boundary. Moreover, the hot electron temperatures, T_e, are obtained from PL spectra to be 6.5, 9, 14, and 16 K for the experimental traces, displayed in Fig. 3(a). These values are used in the calculations. In Fig. 3(b), the temporal evolutions of the spin polarization resulting from calculations with (solid lines) and without the HF term (dashed lines) are compared to the experimental results, showing an excellent agreement with the best fitting parameters. It is noted that the same parameters are used for both calculations with and without the HF term. Obviously, the increase of SDT with increasing P originates from the HF term.

Moreover, we present the temporal evolution of spin polarization with (solid lines) and without (dashed lines) spin-conserving electron-heavy-hole Coulomb scattering in Fig. 3(c). (The detail of electron-heavy hole scattering terms of can be found in Ref. 29.) It is obvious that scattering strength is enhanced while including the spin-conserving electron-heavy-hole scattering. Also the larger the hole density (which increases with the pumped spin polarization) is, the larger the enhancement of scattering strength is. Therefore, the SDT is reduced by the spin-conserving electron-heavy-hole Coulomb scattering. This is consistent with the effect of the scattering in the weak scattering limit.[3] In addition, we have also investigated the effect of the spin-flip electron-heavy-hole Coulomb scattering (the BAP mechanism). We do not present the corresponding figure in this manuscript due to the fact that the BAP mechanism hardly changes the temporal evolution of the spin polarization and can be ignored in our cases as studied by Zhou and Wu recently.[29]

Furthermore, in Fig. 3(d), we show the temporal evolution of spin polarization with (solid lines) and without (dashed lines) the screening from the holes in the screened Coulomb potential under the random-phase approximation (detailed expression can also be found in Ref. 29). There are two mechanisms from the hole screening that influence the spin dephasing. On one hand, the presence of hole screening strengthens the total screening and therefore reduces the electron-electron and electron-hole Coulomb scattering. This

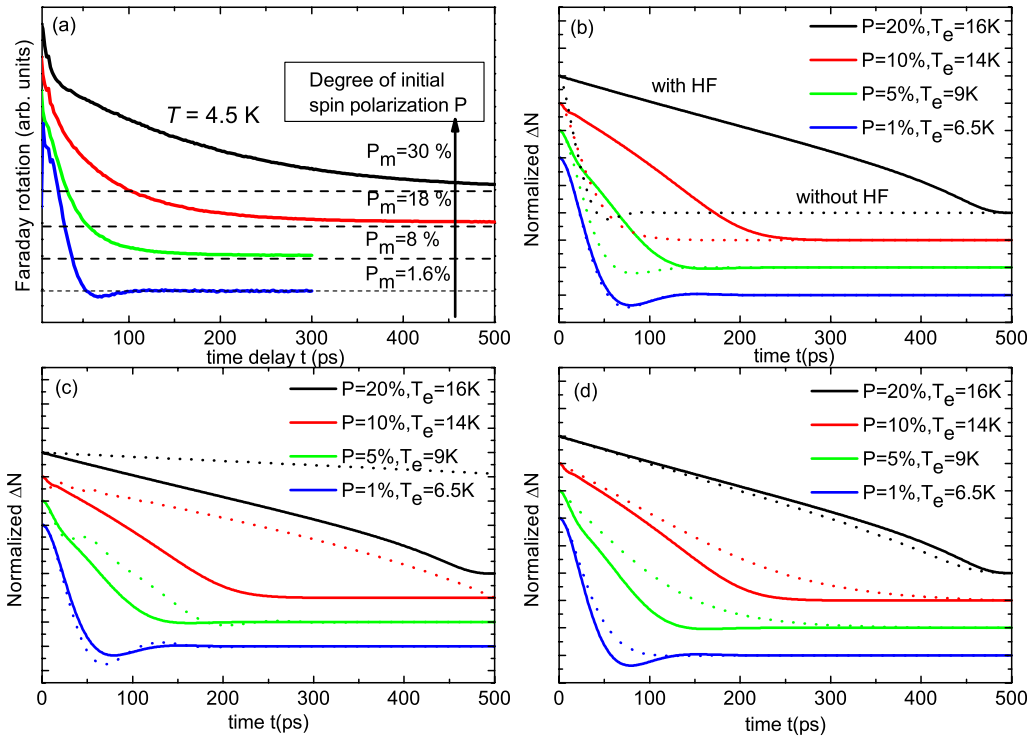

FIG. 3. (Color online) (a) TRFR traces for different pump beam fluences and therefore different initial spin polarizations. P_m is the maximum initial spin polarization calculated from Eq. (2). (b) Calculated spin polarization decay curves for different initial spin polarizations P with (solid curve) and without (dashed curve) HF term. The free parameters in the calculations are the initial spin polarization, and we present the optimal fitting parameters. (c) Calculated spin polarization decay curves with (solid curve) and without (dashed curve) the electron-hole Coulomb scattering. (d) Calculated spin polarization decay curves with (solid curve) and without (dashed curve) the screening from holes.

leads to an increase of the SDT. On the other hand, the presence of hole screening reduces the effect of the HF term. This leads to a reduction of the SDT. The competition between these two mechanisms is clearly shown in the figure: For the lowest spin polarization, the HF term is not important. Therefore, the first mechanism is dominant. For the other three higher polarizations, the HF term is large enough, which leads to the domination of the second mechanism.

In order to verify that the increased SDTs observed in the measurements shown above are due to the increase of the initial spin polarization, instead of either due to the increased electron density or due to the sample heating as the pump beam fluence is increased, measurements with constant excitation density were performed. To vary the degree of initial spin polarization independently of excitation density, the circular polarization degree of the pump beam was adjusted by rotating the $\lambda/4$ plate in the pump beam. The circular polarization degree as a function of the $\lambda/4$ plate angle was measured by using a second $\lambda/4$ plate and a polarizer to analyze the pump beam polarization state.

Figure 4 shows two TRFR traces for low initial spin polarization generated by a nearly linearly polarized pump beam, and high initial spin polarization generated by a circularly polarized pump beam, using the same, high pump beam fluence, and thus resulting in identical electron density and temperature. The traces were normalized to allow for easy comparison. It is clearly visible that the spin dephasing time is longer for the high initial spin polarization case. In Fig. 5(b) the SDTs for a series of measurements with constant, high pump beam fluence and varying initial spin polarization degree are shown, clearly demonstrating an increase of the SDT from less than 200 ps for the low-initial-polarization case to about 300 ps for high initial polarization. They are compared to calculation with and without the HF term. The calculations including the HF term are in excellent agreement with the measured data for both low and high excitation, which again show an increase of the SDT with rising initial spin polarization. If the HF term is excluded

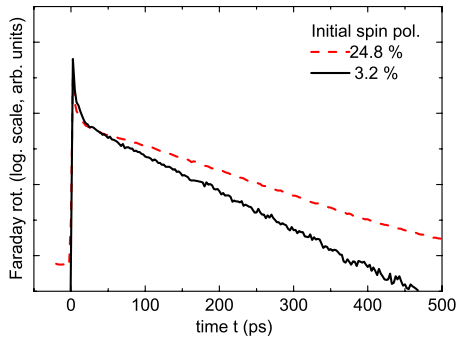

FIG. 4. (Color online) Two TRFR traces for different initial spin polarizations, which were created by varying the circular polarization degree of the pump beam.

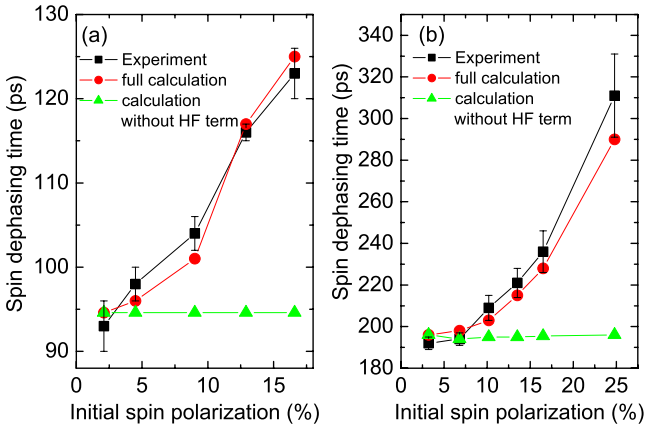

FIG. 5. (Color online) (a) SDTs as a function of initial spin polarization for constant, *low* excitation density and variable polarization degree of the pump beam. The measured spin dephasing times are compared to calculations with and without the HF term, showing its importance. (b) The SDTs measured and calculated for constant, *high* excitation density and variable polarization degree. The values for lowest and highest initial spin polarization correspond to the TRFR traces shown in Fig. 4.

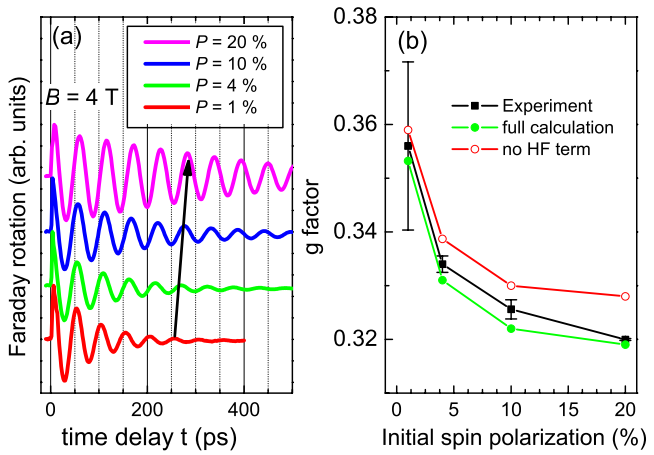

FIG. 6. (Color online) (a) TRFR measurements at B=4 T for different P. An increase of the electron precession period with increasing P is clearly observed (arrow). (b) Comparison of electron g factors for different polarization degrees P, as extracted from the experiments (solid squares), and the calculations with (solid dots) and without (open dots) HF term.

from the calculations, the spin dephasing term is nearly independent of initial spin polarization.

Figure 5(a) compares the SDTs of a second series of measurements with constant excitation densities and variable initial spin polarization to calculations with and without the HF term. In this measurement series, low pump beam fluence, and hence low total carrier density, was used. In the calculation, except for the largest initial spin polarization in each case, there is no fitting parameter. Again, excellent agreements are obtained between the experiment and the theory. Moreover, our results show that the increase of the SDT does solely stem from the HF contribution instead of other effects.

E. Dependence of g factor on initial spin polarization

To determine the electron g factor of the 2D electron system, TRFR measurements with a magnetic field applied within the sample plane were performed (Voigt geometry). The g factor was extracted from the precession frequency as a function of the applied magnetic field. Figure 6(a) shows TRFR traces, taken with a magnetic field of 4 T applied in the sample plane. The pump laser fluence was varied, resulting in different initial spin polarizations and electron densities. With rising initial spin polarization, the effective g factor is reduced by about 10%. In Fig. 6(b), the experimental results are compared to the calculations with and without the HF term, where the same values for the spin polarization as in Fig. 3 were used. The calculations show a similar decrease of the g factor with increasing spin polarization, and the HF term provides only a small correction.

F. Temperature dependence for different initial spin polarizations

Temperature-dependent measurements were performed in a He-flow cryostat in reflection (Kerr) geometry. The SDT, which were determined by fitting a biexponential decay function to the experimental data, are shown in Fig. 7 as a function of temperature for different pump beam intensities, i.e., different spin polarizations P. The theoretical calculations (solid lines of the same color) are in good agreement with the experimental results. We stress that the only fit parameter for each series is the value of the spin polarization, P, which was adjusted to reproduce the experimental data point at highest temperature. Then, the respective temperature dependencies were calculated, keeping P and all other parameters fixed. The hot electron temperatures are taken from the experimental values determined by the intensity-dependent PL measurements. For high pump beam fluence, the electron temperature is significantly higher than the nominal sample temperature, especially for the lower sample temperatures, as Fig. 8 shows. It is clearly visible in Fig. 7 that for the small initial spin polarization, the SDT drastically increases as the sample temperature is raised, for instance, from about 20 ps at 4 K to 200 ps at 50 K for P=0.7%. Re-

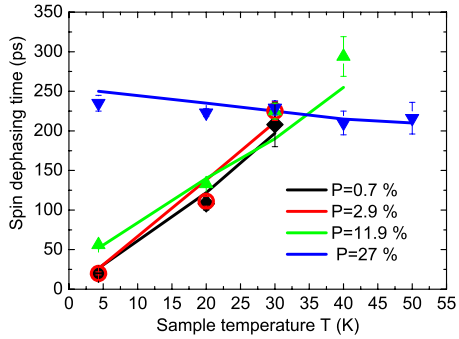

FIG. 7. (Color online) Spin dephasing time as a function of sample temperature, for different initial spin polarizations. The measured data points are represented by solid points, while the calculated data are represented by lines of the same color.

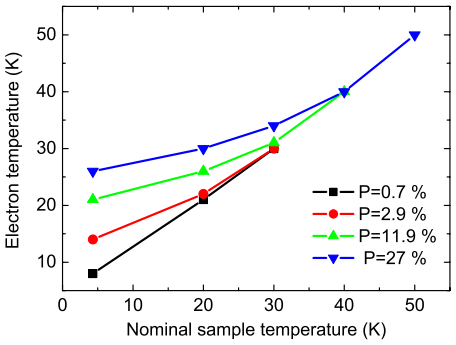

FIG. 8. (Color online) Electron temperature determined from intensity-dependent PL measurements as a function of the nominal sample temperature, for different pump beam fluence and initial spin polarization, under experimental conditions corresponding to the measurements shown in Fig. 7. The measured data points are represented by solid points, while the lines serve as guides to the eye.

markably, for large initial spin polarization, the SDT *decreases* with temperature from about 250 ps at 4 K to a little more than 210 ps at 50 K for $P=16\%$. These features again agree with the theoretical predictions.[10] For small spin polarization, a large increase of the SDT with rising temperature has already been observed by Brand *et al.*[32] This behavior has been discussed from kinetic spin Bloch approach by Weng and Wu[19,33] in the high temperature regime and by Zhou *et al.*[24] in the low-temperature regime. It is due to the increase of the momentum scattering with temperature that leads to the increase of the SDT in the strong scattering limit.[3] For large spin polarization, the decrease of SDT is due to the fact that the effective magnetic field from the HF term decreases with temperature.

V. CONCLUSION

In conclusion, we have performed time-resolved Kerr and Faraday rotation measurements on a high-mobility two-dimensional electron system at low temperatures. We observe that the SDT strongly depends on the initial spin polarization within the sample. This effect is due to the HF term of the electron-electron Coulomb interaction, which serves as an effective magnetic field along the growth axis and inhibits the spin dephasing. By independently varying the degree of initial spin polarization while keeping the excitation density in the experiment constant, we can clearly exclude unrelated origins of the observed increase in spin dephasing time. Furthermore, the contributions of the spin-conserving, spin-flip electron-heavy-hole scattering, and the Coulomb screening from the photo excited hole gas to spin dephasing are studied. The spin-conserving electron-heavy-hole scattering makes the SDT shorter; the spin-flip process can be ignored; and the hole screening makes the SDT larger for small spin polarization and smaller for large ones. Moreover, the electron g factor decreases with increasing spin polarization which is both observed experimentally and reproduced theoretically in the calculations. Finally, we find that the temperature dependence of SDT are very different for small and large spin polarizations. For small spin polarization, the SDT increases with temperature; and for large one, it decreases. Both are in good agreement with the theoretical predictions. In the theory, except for the large initial spin polarization which can not be fully determined from experiment and is treated as fitting parameter, all the other parameters are taken from the experiments. The calculated results fit pretty well with the experimental data. This indicates that the approach based on the kinetic spin Bloch equation can be used in calculating the spin dynamics quantitatively.

ACKNOWLEDGMENTS

We gratefully thank Jaroslav Fabian and R. T. Harley for valuable discussions. This work was supported by the Deutsche Forschungsgemeinschaft via GrK 638, Grant No. Schu1171/1-3, Schu1171/5-1, and SFB 689, the Natural Science Foundation of China under Grant Nos. 10574120 and 10725417, the National Basic Research Program of China under Grant No. 2006CB922005, the Knowledge Innovation Project of Chinese Academy of Sciences and SRFDP. One of the authors (M.W.W.) would like to thank Hailin Wang in University of Oregon, USA, for hospitality where this work was finalized.

*mwwu@ustc.edu.cn
†christian.schueller@physik.uni-regensburg.de

[1] *Semiconductor Spintronics and Quantum Computation*, edited by D. D. Awschalom, D. Loss, and N. Samarth, Nanoscience and Technology (Springer, Berlin, 2002), and references therein.
[2] I. Zutic, J. Fabian, and S. Das Sarma, Rev. Mod. Phys. **76**, 323 (2004), and references therein.
[3] C. Lü, J. L. Cheng, and M. W. Wu, Phys. Rev. B **73**, 125314 (2006).
[4] M. I. D'yakonov and V. I. Perel', Zh. Eksp. Teor. Fiz. **60**, 1954 (1971) [Sov. Phys. JETP **33**, 1053 (1971)].
[5] G. Dresselhaus, Phys. Rev. **100**, 580 (1955).
[6] Y. A. Bychkov and E. I. Rashba, Pis'ma Zh. Eksp. Teor. Fiz. **39**, 66 (1984) [Sov. Phys. JETP **39**, 78 (1984)].
[7] J. M. Kikkawa and D. D. Awschalom, Phys. Rev. Lett. **80**, 4313 (1998).
[8] J. M. Kikkawa, I. P. Smorchkova, N. Samarth, and D. D. Awschalom, Science **277**, 1284 (1997).
[9] J. S. Sandhu, A. P. Heberle, J. J. Baumberg, and J. R. A. Cleaver, Phys. Rev. Lett. **86**, 2150 (2001).
[10] J. Schliemann, J. C. Egues, and D. Loss, Phys. Rev. Lett. **90**, 146801 (2003).
[11] Y. Ohno, R. Terauchi, T. Adachi, F. Matsukura, and H. Ohno, Phys. Rev. Lett. **83**, 4196 (1999).

[12] M. W. Wu and M. Kuwata-Gonokami, Solid State Commun. **121**, 509 (2002).
[13] S. Döhrmann, D. Hägele, J. Rudolph, M. Bichler, D. Schuh, and M. Oestreich, Phys. Rev. Lett. **93**, 147405 (2004).
[14] O. Z. Karimov, G. H. John, R. T. Harley, W. H. Lau, M. E. Flatté, M. Henini, and R. Airey, Phys. Rev. Lett. **91**, 246601 (2003).
[15] M. W. Wu and C. Z. Ning, Eur. Phys. J. B **18**, 373 (2000).
[16] M. W. Wu, J. Phys. Soc. Jpn. **70**, 2195 (2001).
[17] M. Q. Weng and M. W. Wu, Phys. Rev. B **66**, 235109 (2002).
[18] M. M. Glazov and E. L. Ivchenko, JETP Lett. **75**, 403 (2002).
[19] M. Q. Weng and M. W. Wu, Phys. Rev. B **68**, 075312 (2003).
[20] W. J. H. Leyland, G. H. John, R. T. Harley, M. M. Glazov, E. L. Ivchenko, D. A. Ritchie, I. Farrer, A. J. Shields, and M. Henini, Phys. Rev. B **75**, 165309 (2007).
[21] M. W. Wu and H. Metiu, Phys. Rev. B **61**, 2945 (2000).
[22] M. W. Wu, M. Q. Weng, and J. L. Cheng, in *Physics, Chemistry and Application of Nanostructures: Reviews and Short Notes to Nanomeeting 2007*, edited by V. E. Borisenko, V. S. Gurin, and S. V. Gaponenko (World Scientific, Singapore, 2007), pp. 14, and references therein.
[23] M. Q. Weng, M. W. Wu, and L. Jiang, Phys. Rev. B **69**, 245320 (2004).
[24] J. Zhou, J. L. Cheng, and M. W. Wu, Phys. Rev. B **75**, 045305 (2007).
[25] H. Haug and A. P. Jauho, *Quantum Kinetics in Transport and Optics of Semiconductor* (Spinger-Verlag, Berlin, 1996).
[26] M. I. D'yakonov and V. Y. Kachorovskii, Fiz. Tekh. Poluprovodn. (S.-Peterburg) **20**, 178 (1986) [Sov. Phys. Semicond. **20**, 110 (1986)].
[27] *Optical Orientation*, edited by F. Meier and B. P. Zakharchenya (North-Holland, Amsterdam, 1984).
[28] D. Stich, J. H. Jiang, T. Korn, R. Schuh, D. Schuh, W. Wegscheider, M. W. Wu, and C. Schüller, Phys. Rev. B **76**, 073309 (2007).
[29] J. Zhou and M. W. Wu, arXiv:0705.0216 (unpublished).
[30] G. L. Bir, A. G. Aronov, and G. E. Pikus, Zh. Eksp. Teor. Fiz. **69**, 1382 (1975) [Sov. Phys. JETP **42**, 705 (1975)].
[31] S. Pfalz, R. Winkler, T. Nowitzki, D. Reuter, A. D. Wieck, D. Hägele, and M. Oestreich, Phys. Rev. B **71**, 165305 (2005).
[32] M. A. Brand, A. Malinowski, O. Z. Karimov, P. A. Marsden, R. T. Harley, A. J. Shields, D. Sanvitto, D. A. Ritchie, and M. Y. Simmons, Phys. Rev. Lett. **89**, 236601 (2002).
[33] G. Stefanucci and C.-O. Almbladh, Phys. Rev. B **69**, 195318 (2004).
[34] G. Dresselhaus, Phys. Rev. **100**, 580 (1955).
[35] D. Stich, J. Zhou, T. Korn, R. Schulz, D. Schuh, W. Wegscheider, M. W. Wu, and C. Schüller, Phys. Rev. Lett. **98**, 176401 (2007).